Kalman Filter-Based Integration of DGPS and Vehicle Sensors for Localization

Shahram Rezaei, *Member, IEEE*, and Raja Sengupta, *Senior Member, IEEE*

***Abstract*—We present a position estimation scheme for cars based on the integration of Global Positioning System (GPS) with vehicle sensors. The aim is to achieve enough accuracy to enable in vehicle cooperative collision warning, i.e., systems that provides warnings to drivers based on information about the motions of neighboring vehicles obtained by wireless communications from those vehicles, without use of ranging sensors. The vehicle sensors consist of wheel speed sensors, steering angle encoder, and a fiber optic gyro. We fuse these in an extended Kalman filter. The process model is a dynamic bicycle model. We present data from about 60 km of driving in urban environments including stops, intersection turns, U-turns, and lane changes, at both low and high speeds. The data show the filter estimates position, speed, and heading with the accuracies required by cooperative collision warning in all except two kinds of settings. The data also shows GPS and vehicle sensor integration through a bicycle model compares favorably with position estimation by fusing GPS and inertial navigation system (INS) through a kinematic model.**

***Index Terms*—Global Positioning System (GPS), inertial navigation, Kalman filtering, localization, navigation, safety, sensors, vehicles.**

I. Introduction

IN THIS BRIEF, we describe a real-time loosely coupled differential Global Positioning System (DGPS)/vehicle sensors (VS) system integrated by a Kalman filter to estimate the position, heading, and velocity of a car. We use a GPS with a local base station that broadcasts corrections. Hereafter, we say just GPS for simplicity. The VS are six-wheel speed sensors, a steering angle encoder, and an optical yaw rate gyro. The aim is to achieve enough accuracy to enable cooperative collision warning systems (CCW) [1].

The CCW concept provides warnings or situation awareness displays to drivers based on information about the motions of neighboring vehicles obtained by wireless communications from those vehicles, without use of any ranging sensors. Each vehicle is assumed to broadcast information like its position, speed, or heading, periodically. A neighboring vehicle receiving the information differences the received information from its own position to know the relative position or velocity of the sender. This relative information is used to provide collision warnings or advisories to the driver when necessary. Communication is based on dedicated short range communications (DSRC) [2]. The on-board Wi-wireless and GPS equipment has the advantage of being potentially inexpensive compared to the ranging sensors, like radar, required to provide 360° coverage. CCW would also provide information from vehicles that may be occluded from direct line of sight. Reliable position estimation in GPS coordinates is a critical enabling technology for CCW.

Shladover and Tan [3] have derived the accuracies required in position, speed, and heading estimates to produce CCW warnings of reasonable accuracy and consistency. It is useful to resolve position error into longitudinal and lateral components, i.e., along and orthogonal to the lane centerline, respectively. The lateral position errors requirements turn out to be more stringent than the longitudinal error requirement. It is desirable that the standard deviation of the lateral position error stay within 50 cm. Shladover and Tan also describe speed accuracy requirements. Speed errors are expected to stay within 2 m/s. The heading error limits are set by blind spot warning systems. If the heading error is greater than 5°, a vehicle that is behind and in the same lane may be incorrectly assumed to be behind and in the adjacent lane, i.e., in the blind spot.

These numbers represent the system engineering requirements on our position estimator design. It is desirable that these accuracies be maintained in the face of GPS errors and outages. This has been the emphasis of our testing. We have put the system through more than 60 km of testing, much of it in degraded GPS conditions.

We use GPS with a local base station, i.e., DGPS. Our DGPS sensor gives measurements for position, heading, and inertial velocity. Under the best conditions, i.e., eight satellites or more, the GPS error has a standard deviation of about 30 cm. However, when the number of satellites is seven or less due to buildings or trees, the average errors are more than a meter. Moreover, at six satellites or less, the error usually has a bias. Our DGPS is chosen to have an accuracy similar to a wide area surveillance satellite (WAAS) enabled GPS receiver [4].

Results in Section V show the lateral error standard deviation for the positioning system described in this brief, is within the required limits in most, though not all, situations. The situations in which it fails are described as well. We also compare the lateral positions errors against an absolute threshold for reasons described in Section V-A. The heading error stays within the prescribed limits. The results presented are for GPS with an average of six satellites, i.e., average position measurement errors of a meter. It may be noted, that while our testing has focused heavily on degraded GPS conditions, we have not tested in high slip conditions. Our six wheel speed sensors, suitably averaged, deliver accurate inertial speeds in low slip conditions. They are not under high slip conditions [5]. As a matter of fact, we are not using the GPS inertial velocity measurement at all because

Manuscript received May 2, 2006. Manuscript received in final form September 21, 2006. Recommended by Associate Editor R. Rajamani. This work was supported in part by General Motors Research and Development Center under Contract TCS 70709 to the University of California at Berkeley. The views expressed here are those of the authors and not of the research sponsors.

The authors are with the Civil Engineering Department, University of California at Berkeley, Berkeley, CA 94720 USA (e-mail: srezaei@path.berkeley.edu; sengupta@ce.berkeley.edu).

Color versions of one or more of the figures in this paper are available online at http://ieeexplore.ieee.org.

Digital Object Identifier 10.1109/TCST.2006.886439

of its larger delay relative to our wheel speed sensors. Our GPS runs at 5 Hz. The VS runs at 20 Hz.

This brief is organized as follows. The literature review is in Section II. The measurement system is described in Section III. The filter design is given in Section IV. Experimental results are in Section V.

II. Literature Review

There is an extensive literature on estimating the position of land vehicles using GPS ([6]–[22]). We have reviewed it for estimation methodology and the accuracy of position estimates. Since GPS suffers outages and errors, position estimation methods typically fuse GPS with other sensors. Most papers fuse GPS with INS. Two papers, [6] and [7], estimate position like us by fusing GPS with vehicle sensors instead of inertial navigation system (INS). The position estimation systems in these two papers fuse GPS, wheel speed, yaw rate, and an accelerometer. The system in [7] also uses a compass. All these systems are different variants of Kalman filters. The process models are kinematic.

By contrast, we use a bicycle model. This kind of higher order dynamic model has been fused with GPS velocity to estimate slip ([5], [23]–[25]). Other parameters estimated include roll and tire cornering stiffness. By using a dynamic model, we are able to incorporate a steering angle sensor into the position estimation filter. Unlike prior uses of dynamic models, our emphasis is on its use for position estimation, particularly its ability to enhance the robustness of estimates to highly degraded GPS measurements and outage. The results in this brief show the higher order dynamic model results in more accurate position estimates, and greater robustness to GPS error and outage. This is so even though we do not use accelerometers, INS, or carrier-phase GPS. The vehicle sensors we use are present as standard outputs on the controller area network (CAN) bus in most production vehicles. Vehicles with traction control systems also have accelerometers. However, the accelerometer measurements are usually not readable on the vehicle bus. They are embedded inside the traction control component. Our accelerometers were very noisy.

Some papers in the literature record the error in the position estimates they produce. These are summarized in Table I, which lists the type of fusion, the standard deviation of errors, and update rate associated with the DGPS used, the test environment, and the accuracy of the position estimates produced by fusion. The systems in [7]–[9] use carrier phase DGPS. We use the much more widely used and cheaper code-phase DGPS (Ashtech G12). The other systems in Table I use code-phase DGPS. Our positioning accuracies are similar to [10] and [11], though we tested under more degraded GPS conditions. Moreover, the systems in Table I are all based on kinematic models and do not use steering angle measurements. Our system is based on a dynamic model and uses steering angle measurements.

There are a few papers discussing bias and outage in GPS measurements. Solutions such as fuzzy logic [13] and integrated multiple models ([14] and [26]) have been implemented in simulation to address the bias problem. In [14], they change models according to the number of satellites. We found number of satellites does not tell the whole story about the bias in GPS noise. This is because of the geometric dilution of precision (GDOP) effect. When satellites are located at wide angles relative to each other, the possible error margin is small. On the contrary, when satellites are grouped together or located in a line the geometry will be poor and result in bias. References [15]–[17] also discuss GPS outage and attempt to handle it with an accuracy of a few meters. Here, we try to keep accuracy below a meter.

TABLE I
Quantitative Comparison of Estimators in the Literature

	Sensors	GPS accuracy and rate	Test Environment	Positioning Accuracy
This paper	DGPS+VS	0.3 m, 5 Hz	outage	<1m
[7]	DGPS + VS + Accel. + Compass	0.05 m , 2 Hz	no outage	0.02 m
[8]	DGPS + INS	0.05 m, 1 Hz	no outage	<0.02 m
[9]	DGPS+INS	0.05 m, 1 Hz	outage simulation	<0.5 m
[10]	DGPS+INS+ Odometry	0.3 m, 10 Hz	no outage,	<1 m
[11]	DGPS+INS	1 m, 1 Hz	no outage	<1 m
[12]	DGPS+INS	1 m, 1 Hz	no outage	<2 m

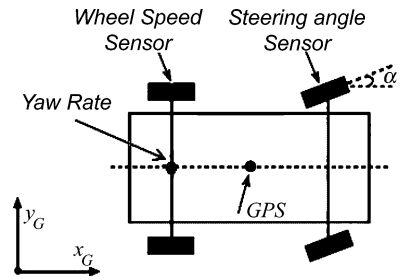

Fig. 1. Vehicle sensors and GPS on the car.

III. Measurement System

Fig. 1 shows the locations of the VS and the GPS on our car. Each wheel has a wheel speed sensor. There are six of them: four for high speeds and two for low speeds. The GPS updates at 5 Hz and the VS updates at 20 Hz.

The steering angle sensor, yaw rate gyro, and wheel speed sensor noises have 1°, 0.3 °/s, and 0.3-m/s standard deviation, respectively, and no bias.

Our GPS gives measurements for position, heading, and inertial velocity. Under the best conditions, i.e., eight satellites or more with line of sight signals, the GPS error has a standard deviation of about 30 cm and no bias. However, when the number of satellites is seven or less due to buildings or trees, the errors are as large as 10 m. Moreover, at six satellites or less, the error usually has a bias in our test areas. Fig. 2 presents the GPS and true trajectory plots from two experiments. One can see the bias in plot (a). Plot (b) shows corruption and outage. We have tried

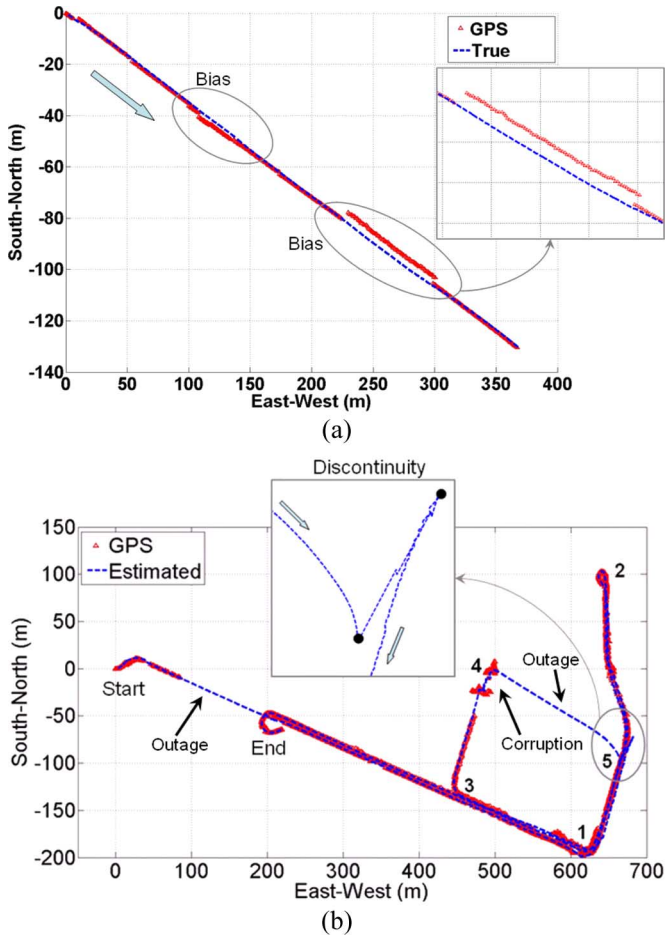

Fig. 2. Typical GPS measurement errors. (a) Bias. (b) Corruption and outage.

to make our filter deliver acceptable accuracy with these kinds of noise.

At low speed, the GPS heading measurement has poor accuracy. It appears completely random when the vehicle stops (see Fig. 15).

IV. Filter Design

Table II describes notations in this section. Fig. 3 shows the layout of our filter. The VS measurements directly drive the process model ("prediction" block). This is used to predict the states of the system at time k based on all measurements till time $k-1$. This prediction is then combined with the GPS measurement in the "update" block to produce the estimate of the states at time k based on measurements up to time k. Our structure follows the filter structure in [28]. In the prediction block, the process model is a bicycle model. Contrary to the commonly used kinematic model which considers the vehicle as a point mass, our bicycle model includes the dimensions of the car, its mass, and moments of inertia. Our state vector is

$$X = [x\ \dot{x}\ y\ \dot{y}\ \phi]^T. \tag{1}$$

All these are estimated in the GPS coordinate system (west–east, south–north) with the origin at the local base station.

TABLE II
Index of Notation:
(not Including Symbols That Are Defined By Formulas)

Notation	*Description*
k	Time index
$\hat{X}$	Vector of Kalman filter states
$\hat{x}, \hat{y}$	West-East and South-North position estimates in the GPS frame, respectively
$\hat{\dot{x}}, \hat{\dot{y}}$	West-East and South-North velocity estimates in the GPS frame, respectively
$\hat{\phi}$	Heading estimate in the GPS frame
Δt	Sampling interval, 50 msec
v	Speed measured by the wheel speed sensor
α	Steering angle
$\dot{\phi}$	Heading rate, measured by the fiber optic gyroscope sensor
x_u, y_u	Longitudinal and lateral displacements between two consecutive timestamps in the body frame, respectively
$\dot{x}_u$, $\dot{y}_u$	Longitudinal and lateral velocities in the body frame, respectively
$\ddot{y}_u$	Lateral acceleration in the body frame
P	Covariance matrix of $\hat{X}$
U	Vector of process model inputs including speed, steering angle, and heading rate
U^m	Vector of speed, steering angle, and heading rate measurements
Q_U	Covariance matrix of noise in the speed, yaw rate, and steering angle measurements
R_{gps}	Covariance matrix of noise in the GPS measurements
$C_{\alpha f}$, $C_{\alpha r}$	Cornering stiffness of the front and rear tires in N/rad, respectively
L_1 , L_2	Longitudinal distances in meters between the center of gravity and front and rear tires, respectively
M	Mass of the vehicle in kg.
I_{zz}	Moment of inertia about the axis normal to plane of motion in kg/m^2

Symbols with 'hat (^)' on top are estimated. Same symbols without hat on top are the true values.

At timestamp k, process model inputs $(v_k, \alpha_k, \dot{\phi}_k)$ are read from the wheel speed, steering angle, and yaw rate sensors, respectively. Then, the bicycle model equations are used to estimate the states at timestamp $k+1$. Equations (2) and (3) (shown at the bottom of the next page) are the prediction equations. Fig. 4 shows the body coordinate frame and displacements in that frame. First, the measurements $(v_k, \alpha_k, \dot{\phi}_k)$ are put into (3) and then the resulting $x_{u(k+1)}$, $\dot{x}_{u(k+1)}$, $y_{u(k+1)}$, and $\dot{y}_{u(k+1)}$ are put into (2). Summarizing (2) and (3) as $X_{k+1/k} = f(X_{k/k}, U(k))$ and $\hat{X}_{k+1/k} = f(\hat{X}_{k/k}, U^m(k))$, where $U^m(k) = (v, \alpha, \dot{\phi})_k$, and linearizing them about $(\hat{X}_{k/k}, U^m(k))$ the covariance matrix $P_{k+1/k}$ of the predicted state is computed by

$$P_{k+1/k} = E\Big(\Big[X^L(k+1/k) - \hat{X}^L(k+1/k)\Big] \times \Big[X^L(k+1/k) - \hat{X}^L(k+1/k)\Big]^T\Big)$$

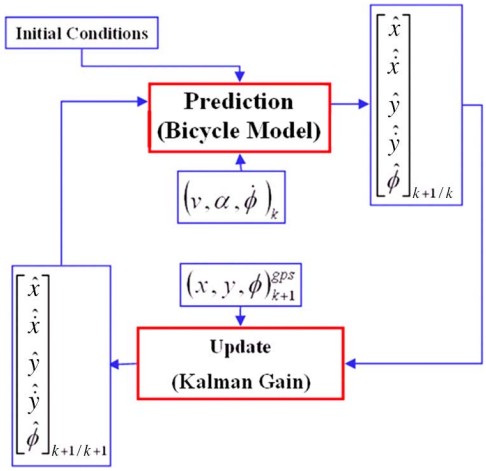

Fig. 3. Layout of the filter.

where

$$X^L(k+1/k) = \left(\frac{\partial f}{\partial X}\right)_{\substack{X=\hat{X}(k/k)\\U=U^m(k)}} \times X^L(k/k) + \left(\frac{\partial f}{\partial U}\right)_{\substack{X=\hat{X}(k+1/k)\\U=U^m(k)}} \times U(k);$$

$$\hat{X}^L(k+1/k) = \left(\frac{\partial f}{\partial X}\right)_{\substack{X=\hat{X}(k/k)\\U=U^m(k)}} \times \hat{X}^L(k/k) + \left(\frac{\partial f}{\partial U}\right)_{\substack{X=\hat{X}(k+1/k)\\U=U^m(k)}} \times U^m(k); \rightarrow$$

$$P_{k+1/k} = \left(\frac{\partial f}{\partial X}\right)_{\substack{X=\hat{X}(k/k)\\U=U^m(k)}} \times P_{k/k} \times \left(\frac{\partial f}{\partial X}\right)^T_{\substack{X=\hat{X}(k/k)\\U=U^m(k)}} + \left(\frac{\partial f}{\partial U}\right)_{\substack{X=\hat{X}(k/k)\\U=U^m(k)}} \times Q_U \times \left(\frac{\partial f}{\partial U}\right)^T_{\substack{X=\hat{X}(k/k)\\U=U^m(k)}} \tag{4}$$

where $\hat{X}(k+1/k) = \hat{X}_{k+1/k}$, $U(k) = U_k$. Since the VS errors are uncorrelated, Q_U is diagonal. Values of the diagonal

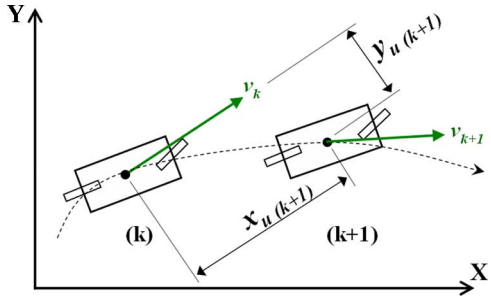

Fig. 4. Body coordinate system on the car.

elements are the variance of the sensor noises, as in the second paragraph of Section III. The update block equations are

$$\begin{aligned}
\hat{X}_{k+1/k+1} &= \hat{X}_{k+1/k} + W_{k+1}\left(Z_{\text{obs}}(k+1) - \hat{X}_{k+1/k}\right)\\
Z_{\text{obs}} &= (x_{\text{gps}}, y_{\text{gps}}, \phi_{\text{gps}})\\
W_{k+1} &= P_{k+1/k}H^T_{k+1}S^{-1}_{k+1}\\
H_{k+1} &= \partial\left([\hat{x}\ \ \hat{y}\ \ \hat{\phi}]^T\right) \Big/ \partial\left([\hat{x}\ \ \dot{\hat{x}}\ \ \hat{y}\ \ \dot{\hat{y}}\ \ \hat{\phi}]^T\right)\Big|_{\hat{X}_{k+1/k}} =\\
H_{k+1} &= \begin{bmatrix} 1 & 0 & 0 & 0 & 0\\ 0 & 1 & 0 & 0 & 0\\ 0 & 0 & 0 & 0 & 1 \end{bmatrix}\\
S_{k+1} &= H_{k+1}P_{k+1/k}H^T_{k+1} + R_{\text{gps}}\\
P_{k+1/k+1} &= P_{k+1/k} - W_{k+1}S_{k+1}W^T_{k+1}
\end{aligned} \tag{5}$$

where R_{gps} is diagonal. The values on the diagonal are the variances of the GPS measurement noises. We have used the following values in the two test environments discussed in Section V

$$R_{\text{gps}} = \begin{bmatrix} 1(m^2) & 0 & 0\\ 0 & 1(m^2) & 0\\ 0 & 0 & 4(\text{deg}^2) \end{bmatrix} \text{RFS}$$

$$R_{\text{gps}} = \begin{bmatrix} 0.04(m^2) & 0 & 0\\ 0 & 0.04(m^2) & 0\\ 0 & 0 & 4(\text{deg}^2) \end{bmatrix} \text{Crows Landing.} \tag{6}$$

$$\begin{bmatrix} \hat{x}\\ \dot{\hat{x}}\\ \hat{y}\\ \dot{\hat{y}}\\ \hat{\phi} \end{bmatrix}_{k+1/k} = \begin{bmatrix} (\hat{x})_{k/k} + \left(x_{u(k+1)}\cos(\hat{\phi}_{k/k}) - y_{u(k+1)}\sin(\hat{\phi}_{k/k})\right)\\ \dot{x}_{u(k+1)}\cos(\hat{\phi}_{k/k}) - \dot{y}_{u(k+1)}\sin(\hat{\phi}_{k/k})\\ (\hat{y})_{k/k} + \left(x_{u(k+1)}\sin(\hat{\phi}_{k/k}) + y_{u(k+1)}\cos(\hat{\phi}_{k/k})\right)\\ \dot{x}_{u(k+1)}\sin(\hat{\phi}_{k/k}) + \dot{y}_{u(k+1)}\cos(\hat{\phi}_{k/k})\\ \hat{\phi}_{k/k} + \dot{\phi}_k\Delta t \end{bmatrix} \tag{2}$$

$$\begin{aligned}
\dot{x}_{u(k)} &= v_{(k)}; \quad \dot{y}_{u(k)} = 0\\
\ddot{y}_{u(k)} &= \left[C_{\alpha f}\left(\alpha_k - \frac{\dot{y}_{u(k)} + L_1\dot{\phi}_k}{\dot{x}_{u(k)}}\right) + C_{\alpha r}\left(-\frac{\dot{y}_{u(k)} - L_2\dot{\phi}_k}{\dot{x}_{u(k)}}\right)\right] \Big/ M\\
\dot{y}_{u(k+1)} &= \ddot{y}_{u(k)}\Delta t, \quad y_{u(k+1)} = \frac{1}{2}\ddot{y}_{u(k)}\Delta t^2\\
\dot{x}_{u(k+1)} &= \dot{x}_{u(k)}, \quad x_{u(k+1)} = \dot{x}_{u(k)}\Delta t
\end{aligned} \tag{3}$$

V. Experimental Results

In this section, we describe our experimental results. Tests have been carried out at the Richmond field station (RFS)[1] and the Crows Landing air field.[2] RFS is an urban environment. The presence of buildings (5–15 m in height) and tall trees (30–60 m) beside the roads create multipath problems. We did tests at RFS with speeds varying between 5 and 25 m/s. The tests included U-turns, stops, right/left turns, and lane changes. In order to test high-speed scenarios, we did tests at Crows Landing. There the multipath problems are insignificant as there is no building or other tall object within a kilometer. The total data set represents more than 60 km of driving (40 km in RFS and 20 km in Crows Landing). The results presented here are either for samples drawn randomly from the data or worst-case behavior.

The main findings we discuss are as follows:

- correct lane discrimination especially under GPS bias or corruption (Section V-A) and outage (Section V-B);
- accuracy of our dynamic model relative to the kinematic model more common in the literature (Section V-B);
- delay in the filter's response to turns including lane change, right/left, and U-turn (Section V-C);
- delay in the filter's response to GPS corrections (Section V-D); and
- accuracy of estimation at low speeds (Section V-E).

Our data shows the filter is able to correctly discriminate the lane of the vehicle except in two kinds of conditions. If GPS is lost or goes bad for a long time (order of 10 s or more) the position errors become large enough to place the vehicle in the wrong lane. The exact duration of outage depends on factors like speed, number of lane changes, etc. The second kind of condition refers to bad GPS during a turn. If GPS is bad during a turn involving a large change of heading, such as a U-turn or an intersection turn, the filter is off on the heading at the end of the turn by a small amount (less than a degree). However, if the GPS remains bad or unavailable after the turn, this small heading error cannot be corrected. It is integrated by the process model eventually resulting in large position errors.

We are able to detect turns and lane changes with delays of the order of 100 ms. It is important to keep this delay small because this filter is a component of on-board safety systems (CCW). Driver reaction time of an unalerted driver is greater than 1 s [27]. We aim to have the system warn the driver within 500 ms or less to avoid the driver perceiving a threat before the system. 100 ms of the 500-ms delay budget is being consumed by the filter. Observe this is two VS sample times. Thus, the filter does not give too much weight to the GPS. It remains sensitive to the accurate and fast VS. At the same time, if GPS is good and there is a big difference between the position estimated by the filter and GPS measurement, we would like the filter to converge fast to the GPS measurement.

The time constant of the response to a GPS step is about 500 ms. Thus, the filter is responding in about 2.5 GPS sample times. It seems it would be hard to get faster while remaining sensitive to the VS for fast response to turns and lane changes. Thus, we feel this filter cannot be tuned to do much better. Significantly enhanced performance would require significantly different design.

[1]RFS is part of the University of California at Berkeley and is located in Richmond, CA.

[2]Crows Landing is affiliated to NASA and located near Patterson, CA.

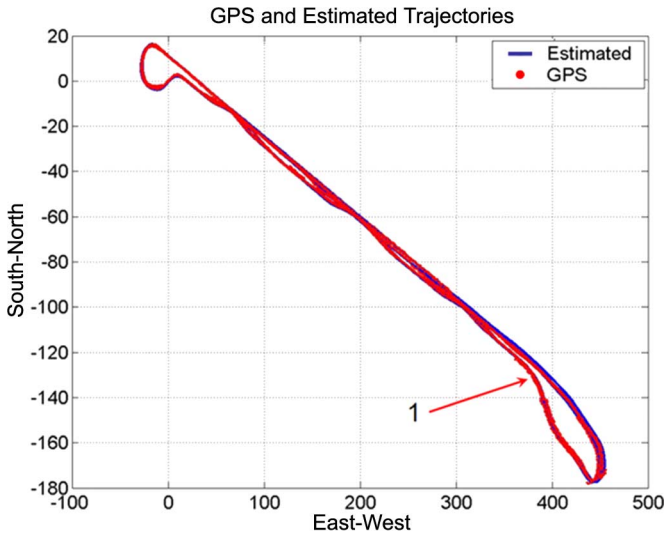

Fig. 5. Car is traveling between two sides of a two-way straight road for the purpose of lane discrimination examination.

A. Lane Discrimination

Fig. 5 shows the estimated trajectory of the car and the raw GPS plot during a test done at RFS. Positions are in the GPS coordinate system. The road is a straight two-way road with one lane each way. The true positions of the lane centerlines in the GPS coordinate system have been determined beforehand through repeated measurement. The car starts at (0,0) and goes to the other end of the road while doing some lane changes on the way. The test driver attempts to keep the center of the car on the center of the lane when going straight. At the end of the road, the car makes a U-turn and returns to the starting position by driving straight. It then makes a U-turn to repeat the pattern. This loop is traveled thirty times.

Along the road, there are trees and buildings that deteriorate the GPS signal. The variation in the number of satellites is shown in Fig. 6. This road is at RFS, i.e., is a small office campus. The average number of satellites during this run is about six. With six satellites, our GPS position readings usually have more than 1 m error.

We first discuss lane discrimination when the vehicle is driving straight. The lateral position error is shown in Fig. 7 for the return legs (there are thirty of them) of the drive shown in Fig. 5. Recall, the car drives straight back to the starting point during the return. The lateral position error is the deviation of the car from the center of the lane in the direction normal to the centerline of the lane. The standard deviation of the lateral position error for the data in Fig. 7 is 0.3 m. The CCW standard deviation requirement is 0.5 m [3].

The "lane boundary" lines in the figure are at ± 90 cm. The standard width of a lane is 3.6 m and the width of the car is about 1.8 m, so if the center of the car is off by more than 90 cm from the center of the lane, it would be considered to be partly in the next lane. This could activate a warning signaling a vehicle in

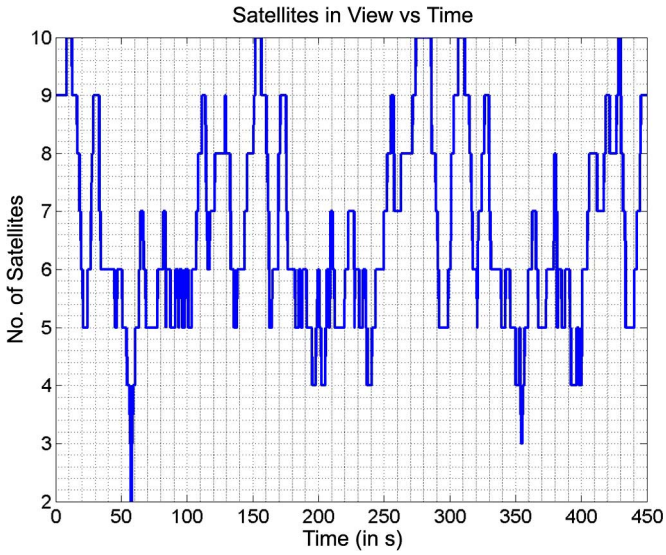

Fig. 6. Variation of number of satellites versus time.

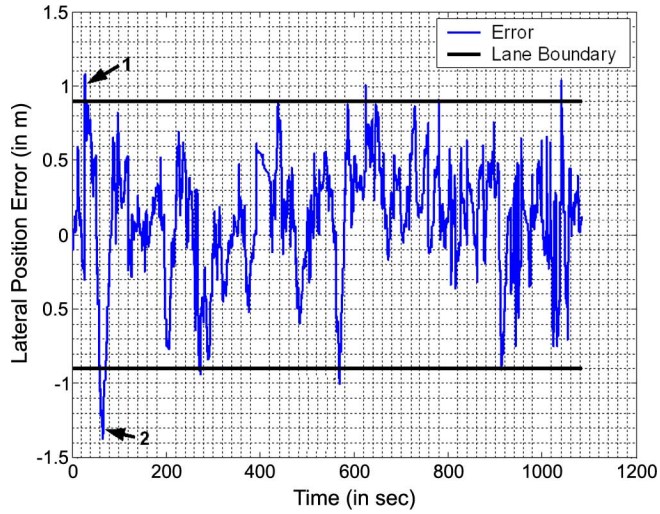

Fig. 7. Lateral position error of the car, this data corresponds to 15 km of driving.

the next lane, when there is none. Note some of this error is due to the test driver.

There are a few points at which the filter error crosses the ± 90 cm boundary. We discuss two of them since the reasons leading to these deviations are representative of all the other cases we have observed. The points are plotted at high resolution in Fig. 8. It shows the lateral position error of the car in the road frame versus time. The number of satellites is also shown. Large errors occur at points 1 and 2 for the two reasons described in the third paragraph of this section. Point 1 occurs after a U-turn. Fig. 6 shows GPS is also bad at the same time. Adding digital map information to the filter may address this problem. However, maps of the required accuracy are not yet a commercial reality. At point 2, continuous bad GPS (more than 20 s) sends the filter in the wrong direction.

Fig. 9 is a plot of error in our heading estimates for the same data used to generate Fig. 7. It shows heading error is always within $\pm 5^{\circ}$ which is one of the requirements.

The bias in GPS position outputs is hard to handle with the filter. Fig. 10 shows the results of an experimental test at RFS.

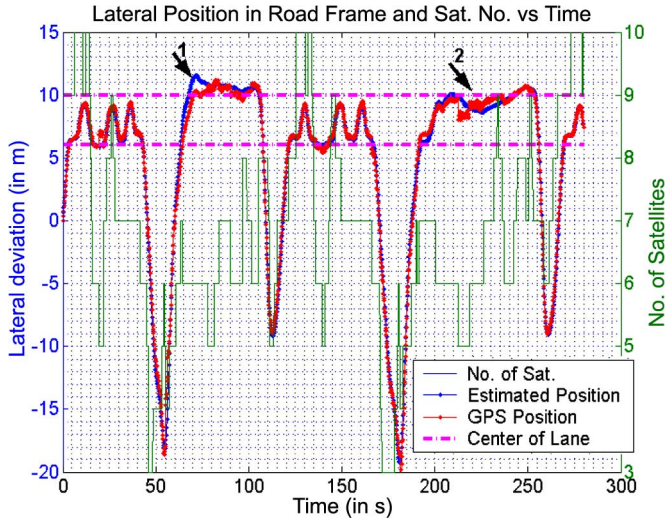

Fig. 8. Lateral position in the road frame as well as number of satellites versus time for the points marked in Fig. 7.

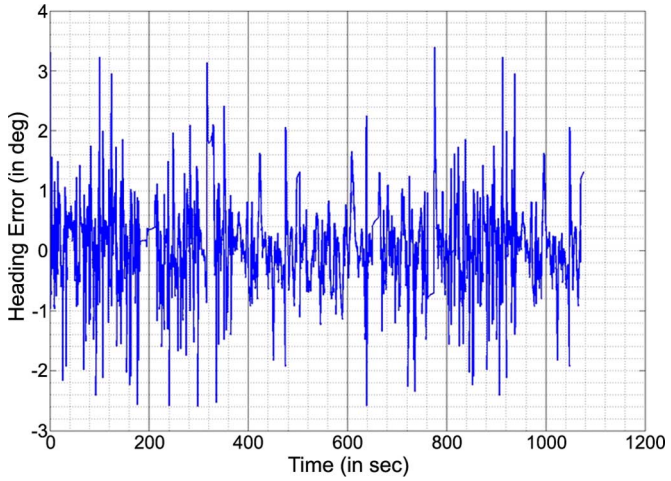

Fig. 9. Heading estimation error versus time.

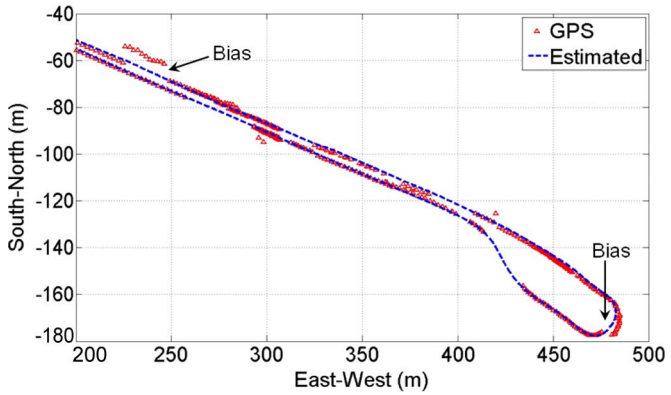

Fig. 10. Bias in GPS noise is handled by the estimator.

At the marked zones, we observed 2–5-m bias in GPS lateral position. The estimator follows the true path. However, the bias will eventually pull the estimator in the wrong direction if it lasts long enough.

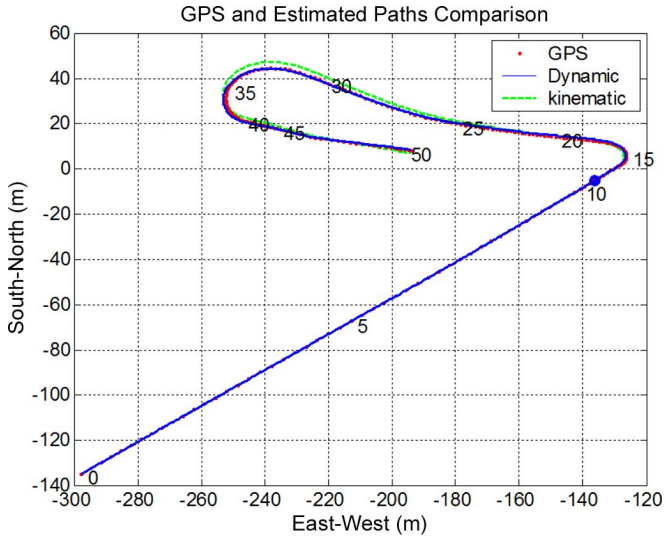

Fig. 11. Trajectory plot for a left turn using kinematic and dynamic process models.

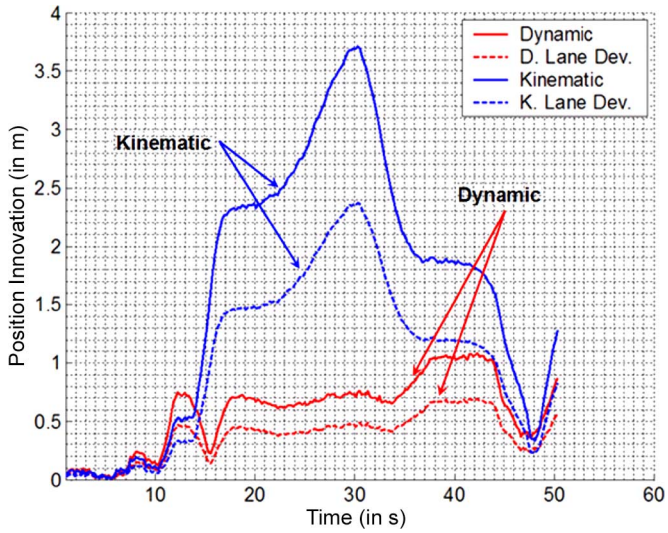

Fig. 12. Innovation plot for the run of Fig. 11.

B. Comparison of Process Model, GPS Outage

In this section, we compare the performance of our dynamic model to the kinematic model common in the literature. We show this by simulating the GPS outage problem. Fig. 11 shows the trajectory plot for a run, including a left turn, carried out at Crows Landing. The GPS path is very accurate (less than 20-cm error from the true path), because GPS coverage is good throughout this run. We consider the GPS path as the true path. Estimated trajectories, as computed by integrating both dynamic and kinematic process models, are also shown. GPS updates are cut deliberately after 10 s. The VS data continues to flow to the filter. Thus, the filters are running open loop (just by running the dynamic or kinematic model) after 10 s.

Fig. 12 presents the absolute innovation (the Euclidean distance between the point on GPS path and the corresponding point on the estimated path) and lateral position error versus time. Lateral error is computed by projecting the innovation on the direction normal to the heading of the car. The dynamic model does better. Its lateral error is below the lane boundary even though the outage is more than 30 s long. In fact, the kinematic model does not see the inertial delay and as a result, during turns it turns earlier and causes error. In this run, the speed is about 20 m/s when going straight and 10 m/s during the turn. Similarly, the curves for total position error show the dynamic model does better.

We also did many tests during which the car just goes straight and there is a GPS outage. The open-loop system diverges from the true path as expected. Consistently, the dynamic model diverges less.

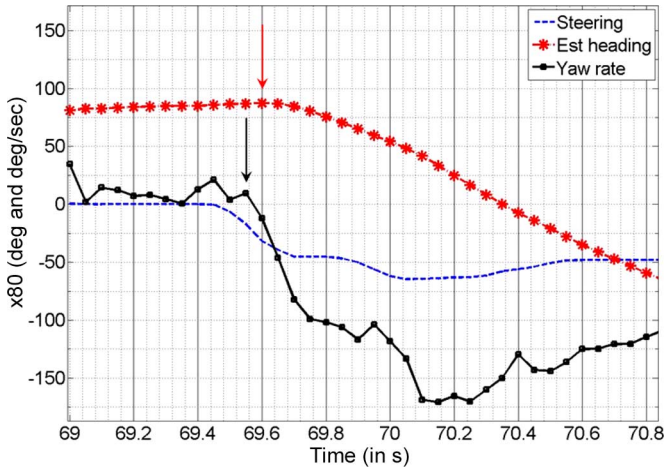

Fig. 13. Delay in response to turn for point 1 in Fig. 5.

C. Delay in Response to Turn

We illustrate the delay exhibited by the filter in responding to a turn by using the test in Fig. 5. We focus on one point, point 1 (shown with an arrow on Fig. 5). We compare the true starting time of the turn and the starting time as determined from the heading output of the filter (see Fig. 13). In Fig. 13, steering angle, heading deviation from 20°, and yaw rate values are scaled by 80.

We assume the true starting time of the turn (shown with an arrow in Fig. 5) is when there is an increase in absolute value of yaw rate measured by the yaw rate sensor. We know this to a precision of 50 ms. The steering angle plot may also be used to determine the true time. The heading estimated by the filter starts responding within 100 ms. The delays observed in the rest of our data are similar. The response delay of the filter to a turn is about 100 ms. At point 1, the number of satellites is just 3 and at point 2 it is 7. Hence, the delay is not related to GPS quality. This is because we have a good process model and heading is predicted directly using the yaw rate sensor output.

D. Delay in Response to GPS Correction

We are interested in the response delay to GPS inputs. When GPS is good we would like the filter to converge fast to the GPS readings. We illustrate the response of our filter using the test run in Fig. 2(b). Numbers on the figure mark different zones visited during the trip. This test was executed at RFS. The car travels from the start point (0,0) toward zone 1, then to 2, makes a U-turn there, then comes back to 1. From 1, the car travels

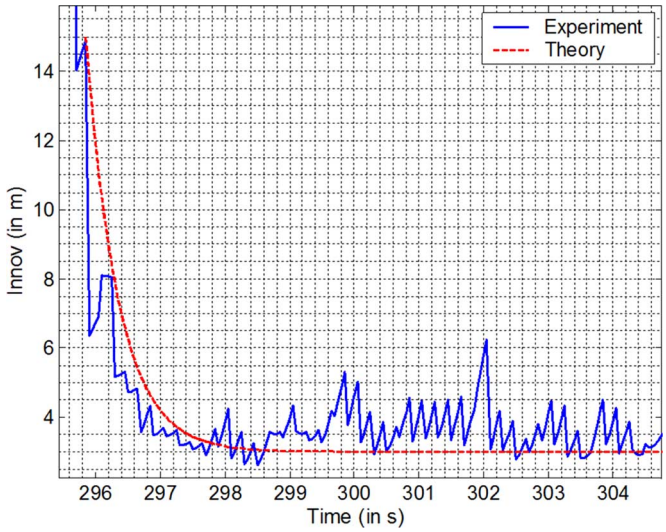

Fig. 14. Comparison of experimental step input response and a first-order model with time constant 500 ms.

along a loop by passing zones 3–5. Finishing the loop, the car goes to the end point and stops there. Timing information of turning points are as follows (some zones are visited multiple times):

Point	Time(s)		Point	Time(s)
1	90, 210, 315		4	270
2	160		5	105, 190, 295
3	65, 230, 330			

The average number of satellites for this run is less than 5, which means average GPS position errors worse than 2–3 m. To see the misleading effect of bad GPS readings, consider the portion of time the car travels along the loop, particularly on the part connecting 3 to 4 and 5 (between 210 and 300 s). GPS outage before and after 4 together with faulty observations at 4 mean the filter is essentially running open loop with bad initial conditions. This causes divergence from the true path and significant error. The discontinuity in the estimated path at zone 5 is due to this. Fig. 14 plots the data right after GPS data becomes good in zone 5. On reaching good GPS coverage, the filter removes the error using the GPS observations. The solid line in Fig. 14 plots innovation, i.e., the difference between the GPS measurement and the filter position output. One can see the filter is stable. The dashed line is the step response of a first-order system with a time constant of 500 ms. The dashed curve has been a good fit to all the data we have analyzed. Thus, the filter time constant seems to be about 500 ms or about 2.5 GPS sample times. The filter appears to reduce error reasonably fast.

E. Low Speed

GPS heading is very poor at low speeds and it appears completely random when the vehicle stops. Nevertheless our data shows our filter is able to compensate for this. The RFS runs are almost all with the vehicle traveling under 15 m/s. It starts and stops frequently. The filter is able to maintain accurate tracks even as the vehicle stops and starts. Fig. 15 shows GPS and estimator heading error versus time when the vehicle is at a stop sign. The stop sign is located on the trajectory in Fig. 5. As seen, when the vehicle stops, the GPS heading error reaches 160°. However, the estimator heading estimate remains within ±5°.

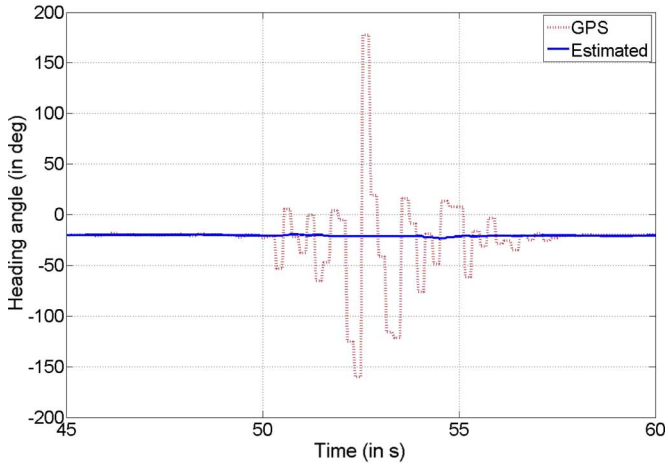

Fig. 15. GPS heading measurements have higher error in low speed.

VI. Conclusion

In this brief, we discussed a real time position estimator, designed and implemented on cars. An extended Kalman filter integrated vehicle sensors including wheel speed, yaw rate gyro, and steering angle with DGPS observations. A dynamic bicycle model was used as the process model in order to enhance the performance at high speeds and during fast turns. We analyzed the performance of the filter using about 60 km of experimental tests carried out in environments with good and bad GPS coverage. The filter is designed to enable CCW systems. The data indicates it can meet CCW requirements in many but not all circumstances.

Acknowledgment

The authors would like to thank Dr. H. Krishnan of General Motors for his suggestions on the design of the filter. They would also like to thank Dr. H. Tan and Dr. Q. Xu of the PATH program. Dr. Tan suggested they use the bicycle model. Dr. Xu helped them debug the filter once they started testing it. They would also like to thank Dr. S. Dickey, D. Nelson, and S. K. Tan for helping with implementing the filter on the Buicks and the many weeks of work that gave them their experimental data. They also thank General Motors Inc. for their sponsorship.

References

[1] R. Sengupta, S. Rezaei, S. E. Shladover, J. A. Misener, S. Dickey, and H. Krishnan, "Cooperative collision warning systems: Concept definition and experimental implementation," *J. Intell. Transport. Syst.*, vol. 11, no. 3, pp. 143–155, 2007.

[2] Q. Xu, J. Ko, T. Mak, and R. Sengupta, "Protocol design for vehicle-vehicle safety messages," *IEEE Trans. Veh. Technol.*, to be published.

[3] S. E. Shladover and S.-K. Tan, "Analysis of vehicle positioning accuracy requirements for communication—based cooperative collision warning," *J. Intell. Transport. Syst.*, vol. 10, no. 3, pp. 131–140, 2006.

[4] S. Pullen, T. Walter, and P. Enge, "System overview, recent developments, and future outlook for WAAS and LAAS," in *Proc. Tokyo Univ. Mercantile Marine GPS Symp.*, 2002, pp. 45–56 [Online]. Available: http://waas.stanford.edu/pubs/index.htm

[5] D. M. Bevly, J. C. Gerdes, C. Wilson, and G. Zhang, "The use of GPS based velocity measurements for improved vehicle state estimation," in *Proc. Amer. Contr. Conf.*, 2000, pp. 2538–2542.

[6] W. W. Kao, "Integration of GPS and dead-reckoning navigation systems," in *Proc. IEEE Veh. Navig. Inf. Syst. Conf.*, 1991, pp. 635–643.

[7] D. Hohman and T. Murdock *et al.*, "GPS roadside integrated precision positioning system," in *Proc. IEEE Position Location Navig. Symp.*, 2000, pp. 221–230.

[8] J. Farrell, "Real-time differential carrier phase GPS-aided INS," *IEEE Trans. Contr. Syst. Technol.*, vol. 8, no. 4, pp. 709–721, Jul. 2000.

[9] R. M. Rogers and J. S. Wit *et al.*, "Integrated INU/DGPS for autonomous vehicle navigation," in *Proc. IEEE Position Location Navig. Symp.*, 1996, pp. 471–476.

[10] I. Abuhadrous, F. Nashashibi, C. Laurgeau, and M. Chinchole, "Multisensor data fusion for land vehicle localization using RTMAPS," in *Proc. IEEE Intell. Veh. Symp.*, 2003, pp. 339–344.

[11] J. P. Wang, W. F. Tian, and Z. H. Jin, "Study on integrated micro inertial navigation system/GPS for land vehicles," in *Proc. IEEE Intell. Transport. Syst.*, 2003, pp. 1650–1653.

[12] K. A. Redmill, T. Kitajima, and U. Ozguner, "DGPS/INS integrated positioning for control of automated vehicle," in *Proc. IEEE Intell. Transport. Syst.*, 2001, pp. 172–178.

[13] S. R. Swanson, "A fuzzy navigational state estimator for GPS/INS integration," in *Proc. IEEE Position Location Navig. Symp.*, 1998, pp. 541–548.

[14] D. Huang and H. Leung, "EM-IMM based land-vehicle navigation with GPS/INS," in *Proc. IEEE Intell. Transport. Syst.*, 2004, pp. 624–629.

[15] W. Lipp, V. Sagrestani, and R. Sarrica, "Integrated GPS/fiber optic gyro land navigation system," in *Proc. IEEE Position Location Navig. Symp.*, 1994, pp. 447–452.

[16] S. Weisenburger and C. Wilson, "An integrated vehicle positioning system for safety applications," *J. Navig.*, vol. 47, no. 2, pp. 75–81, 2000.

[17] M. Imamura, K. Kobayashi, and K. Watanabe, "Real time positioning by fusing differential GPS and local vehicle sensors," in *Proc. IEEE/SICE*, 2003, pp. 778–781.

[18] C. Hide, T. Moore, and M. Smith, "Adaptive Kalman filtering algorithms for integrating GPS and low cost INS," in *Proc. IEEE Position Location Navig. Symp.*, 2004, pp. 227–233.

[19] W. Li and H. Leung, "Constrained unscented Kalman filter based fusion of GPS/INS/digital map for vehicle localization," in *Proc. IEEE Intell. Transport. Syst.*, 2003, pp. 1362–1367.

[20] K. P. Schwarz, M. Wei, and M. Van Gelderen, "Aided versus embedded—a comparison of two approaches to GPS/INS integration," in *Proc. IEEE Position Location Navig. Symp.*, 1994, pp. 314–322.

[21] Q. Honghui and J. B. Moore, "Direct Kalman filtering approach for GPS/INS integration," *IEEE Trans. Aerosp. Electron. Syst.*, vol. 38, no. 2, pp. 687–693, Apr. 2002.

[22] S. Panzieri, F. Pascucci, and G. Ulivi, "An outdoor navigation system using GPS and inertial platform," *IEEE/ASME Trans. Mechatronics*, vol. 7, no. 2, pp. 134–142, Jun. 2002.

[23] J. Ryu and J. C. Gerdes, "Estimation of vehicle roll and road bank angle," in *Proc. Amer. Contr. Conf.*, 2004, pp. 2110–2115.

[24] P. Yih, J. Ryu, and J. C. Gerdes, "Vehicle state estimation using steering torque," in *Proc. Amer. Contr.Conf.*, 2004, pp. 2116–2121.

[25] D. M. Bevly, R. Sheridan, and J. C. Gerdes, "Integrating INS sensors with GPS velocity measurements for continuous estimation of vehicle sideslip and tire cornering stiffness," in *Proc. Amer. Contr. Conf.*, 2001, pp. 25–30.

[26] E. Mazor, A. Averbuch, Y. Bar-Shalom, and J. Dayan, "Interacting multiple model methods in target tracking: A survey," *IEEE Trans. Aerosp. Electron. Syst.*, vol. 34, no. 1, pp. 103–123, Jan. 1998.

[27] J. Carbaugh, D. N. Godbole, and R. Sengupta, "Safety and capacity analysis of automated and manual highway systems," *Transport. Res. Part C (Emerging Technol.)*, vol. 6C, no. 1–2, pp. 69–99, 1998.

[28] J. Guivant, E. Nebot, and S. Baiker, "Autonomous navigation and map building using laser range sensors in outdoor applications," *J. Robotic Syst.*, vol. 17, no. 10, pp. 565–283, 2000.